Optical properties and quantum efficiency of thin-film alkali halides in the far ultraviolet

Juan I. Larruquert, José A. Méndez, José A. Aznárez, Anton S. Tremsin, and Oswald H. W. Siegmund

The optical constants of thin films of CsI, KI, and KBr and the quantum efficiency (QE) of planar photocathodes made with these alkali halides in the 53.6–174.4-nm spectral range are presented. The optical constants were obtained from measurements of the reflectance as a function of incidence angle. The effect of film heating and exposure to UV irradiation on the optical properties and on the QE of the three alkali halides was investigated. KBr was found to be the most stable material for both heating and UV irradiation. KI appeared to be close to temperature stable, whereas UV exposure affected its optical constants. CsI optical constants changed after 420 K heating and after UV exposure. The changes in the optical constants were related to the QE changes, and a certain correlation between both variations was determined. However, it was also demonstrated that the QE changes cannot be explained solely by the changes in optical constants.

OCIS codes: 260.7200, 260.7210, 120.4530.

1. Introduction

The photocathodes made with alkali halides have attracted considerable interest in recent years, as they provide an efficient means for UV photon conversion over a wide spectral range of the extreme-UV (EUV, $10\ \text{nm} < \lambda < 100\ \text{nm}$) and far-UV (FUV, $100\ \text{nm} < \lambda < 200\ \text{nm}$) radiation. Among these materials, thin films of CsI, KI, and KBr exhibit relatively high quantum-efficiency (QE) values and, therefore, are extensively used in EUV and FUV detection devices. The optical characterization of films of the above materials in the EUV and FUV spectral range is necessary for optimization of the QE of photocathodes made with these films.

The optical constants of single crystals of CsI (Ref. 1; for wavelengths longer than 112.7 nm), KI (Refs. 2–5; for wavelengths longer than 35.4 nm), and KBr (Refs. 6 and 7; for wavelengths longer than 31.0 nm) have been described in the literature. However, in the EUV and FUV spectral range thin films of these materials have not yet been fully characterized. Eby *et al.*,[8] Teegarden and Baldini,[9] and Saito *et al.*[10] performed absorption measurements for many alkali-halide thin films, although neither optical constants nor absorption coefficients were determined. Lu and McDonald[11] measured CsI thin-film transmittance at wavelengths longer than 115 nm. They used an unspecified approximation to obtain the absorption length from transmittance measurements. Boutboul *et al.*[12] published absorption-length data for thin films of CsI, KI, and other alkali iodides in the 140–220-nm spectral range.

Here we report *in vacuo* room-temperature measurements of the reflectance and the optical constants of as-deposited, as well as annealed to 420 K, and UV-irradiated thin films of CsI, KI, and KBr. The measurements were performed in the 53.6–174.4-nm spectral range. We also directly measured the changes in QE of planar photocathodes made with the three materials. We calculated their QE variations by using the measured values of the reflectance and the optical constants and by assuming that the photoelectron transport properties remain unchanged after treatment. The measured and calculated values of QE variation were then compared.

2. Experimental Techniques

A. Thin-Film Optical Characterization

Thin-film deposition, EUV and FUV reflectance measurements, and sample treatments were performed

J. I. Larruquert (larruquert@io.csic.es), J. A. Méndez, and J. A. Aznárez are with the Instituto de Fisica Aplicada, Consejo Superior de Investigaciones Cientificas, 28006 Madrid, Spain. A. S. Tremsin and O. H. W. Siegmund are with the Space Sciences Laboratory, University of California at Berkeley, Centennial Drive at Grizzly Peak Boulevard, Berkeley, California 94720-7450.

Received 10 July 2001; revised manuscript received 19 December 2001.

0003-6935/02/132532-09$15.00/0

in the Metal Optics Laboratory at Instituto de Física Aplicada, Consejo Superior de Investigaciones Cientificas (CSIC) by use of a reflectometry–deposition system that has been described elsewhere.[13,14] The reflectometer is equipped for *in situ* UHV thin-film deposition and allows for reflectance measurements in the 50–200-nm spectral range for incidence angles that vary from near normal to near grazing. The system contains three connected vacuum chambers: a sample transfer chamber, a deposition chamber, and a reflectometry chamber.

In the deposition chamber the alkali halides were sublimated from Ta boats provided with a Chromel–Alumel (K type) thermocouple to control the temperature. The sublimation temperature was always maintained below the melting point to minimize the possibility of dissociation of the compounds. We used 99.999% purity powder CsI, KI, and KBr. The film thickness was calibrated by use of Tolansky interferometry. The deposition process for CsI was performed at a rate of approximately 4 nm/s, and the rate for KI and KBr was approximately 1.2 nm/s.

The base pressure in the reflectometer chamber (when isolated from the lamp and the monochromator) was 2×10^{-8} Pa. Typical pressures at different experimental stages comprised approximately 5×10^{-6} Pa in the deposition chamber during alkali-halide deposition, 10^{-6} Pa during sample heating, 10^{-5} Pa during UV exposure, and 3×10^{-7} Pa during reflectance measurements. The residual gas in the reflectance measurement chamber consisted mainly of a nonoxidizing gas mixture (93% He, 3% Ne, 3% Ar, and 1% N_2) that flowed in the discharge lamp, a small fraction of which reached the UHV reflectometer chamber through several differential pumping arrangements. The above mixture of gases was used to have a discharge with the spectral lines of the four gases at a time. The reflectance measurements were performed at room temperature (~300 K).

We performed UV irradiation of the sample in the sample transfer chamber using an Oriel 200-W, Hg–Xe lamp placed in front of a MgF_2 window. The lamp was calibrated and provided a radiation flux on the sample of 4.3×10^{-7} W/mm^2, which corresponds to 5.5×10^{11} photons/mm^2/s at the 253.7-nm Hg line.

The sample treatments and reflectance measurements were performed as follows. First, a thin film of an alkali halide was deposited onto a 50.8 mm × 50.8 mm × 3 mm float glass substrate. After deposition, the sample was transferred to the reflectometer chamber, and its reflectance was measured in the 53.6–174.4-nm spectral range for several incidence angles. The sample was then transferred back to the treatment chamber for each annealing or UV irradiation treatment and returned to the reflectometry chamber for new reflectance measurements. After heat treatment the sample was allowed to cool down to room temperature before new reflectance measurements were performed. All the above procedures were carried out without breaking vacuum.

B. Photocathode Preparation and Characterization

The efficiency of photoconversion of CsI, KI, and KBr films was characterized with flat reflective photocathodes in the Space Sciences Laboratory at the University of California at Berkeley. We deposited ≈800-nm-thick films of CsI, KI, and KBr by sublimation on polished stainless-steel substrates (4 cm × 4 cm) at a rate of ≤2.0 nm/s and at pressures ~2.6×10^{-4} Pa. The samples were prepared in conditions as similar as possible to those prepared at CSIC for reflectance measurements, within the differences of the two experimental setups. After deposition, the chamber was purged with dry nitrogen and all the samples were then briefly exposed to air (~6 min) during their transfer from the deposition station to the QE measurement vacuum chamber. The samples were mounted on the front face of a custom-made electrometer, which allowed us to measure the photocurrent from the photocathodes with an accuracy of approximately 0.5 fA. A positively biased mesh was positioned 3 mm in front of the photocathodes to provide efficient photoelectron collection. All the QE measurements reported in this section were performed at normal incidence. The quantum efficiencies of the photocathodes were measured with monochromatic radiation provided by a gas-discharge, hollow-cathode source in combination with a 1-m grazing-incidence monochromator. The absolute QE data were derived from the flux-measurement comparisons with a reference standard: National Institute of Standards and Technology (NIST)-calibrated EUV (windowless) and FUV (sealed) photodiodes. The spectral response of the as-deposited photocathodes was measured several hours after deposition and then remeasured after heat treatment and UV exposure. Heat treatment and UV exposure of the samples were performed *in situ* and did not require breaking vacuum. The UV radiation for the study of the sample aging was provided by a mercury-vapor, pen-ray lamp installed in the chamber at a distance of ~0.5 m from the samples. The incident photon flux from the lamp at the plane of the samples was measured to be 1.15×10^{10} and 4×10^8 photons/mm^2/s for 253.7- and 184-nm wavelengths, respectively. The thermally treated samples were heated from the rear side with a resistive heater to temperatures of approximately 370 K for 4–6 h and then allowed to cool to room temperature over a period of several hours.

3. Reflectance Measurements and Optical Constants of the Three Alkali Halides

The reflectance measurements for the thin films of the three materials were performed at nine incidence angles that varied from 5° to 80° within the horizontal plane of incidence of the reflectometer. These measurements were used to obtain the optical constants of the films. We calculated the optical constants by minimizing the following merit function:

$$S_j^2 = \sum_{i=1,\ldots,9} \{R^{\exp}_{\theta_i} - R[\theta_i, n_j, k_j, p]\}^2, \qquad (1)$$

where $R^{\exp}_{\theta_i}$ is the reflectance measured at the incidence angle of θ_i, and $R[\theta_i, n_j, k_j, p]$ is the calculated reflectance for the trial set (n_j, k_j) of optical constants at the jth iteration and for the degree of polarization of beam p, which will be defined below. The amplitude reflectance of the multilayer vacuum–thin-film–glass substrate for s and p polarization is given by

$$r^{s,p} = \frac{r_{12}^{s,p} + r_{23}^{s,p} \exp(2i\beta)}{1 + r_{12}^{s,p} r_{23}^{s,p} \exp(2i\beta)}, \quad (2)$$

where $r_{ij}^{s,p}$ are the well-known Fresnel reflection coefficients at interface ij for incoming radiation with parallel (p) or perpendicular (s) electric vectors, respectively; 1 stands for vacuum; 2 represents the thin film; and 3 represents the substrate. β is a complex function given by

$$\beta = k_0 x (n_2^2 - n_1^2 \sin^2 \theta)^{1/2}, \quad (3)$$

where θ is the incidence angle of the beam, x is the film thickness, n_1 is the refractive index of the incidence medium, n_2 is the complex refractive index of the thin film, and k_0 is the free-space wave vector.

Radiation that entered the reflectometer chamber was partially polarized. The degree of polarization is defined as

$$p = (I_p - I_s)/(I_p + I_s), \quad (4)$$

where I_p and I_s are the intensities of the incident radiation with the electric vector parallel and perpendicular, respectively, to the incidence plane. p was a known, wavelength-dependent parameter of the monochromator, which had been determined previously along with the optical constants of the glass substrates, which were also used in the calculation of the optical constants of the alkali halides. The reflectance of the multilayer vacuum–thin-film–glass substrate is given by

$$R = \frac{1 + p}{2} R_p + \frac{1 - p}{2} R_s, \quad (5)$$

where R_p and R_s are the intensity reflectance for p and s polarization, respectively. They are equal to the square modulus of the amplitude reflectance for the parallel and perpendicular electric vectors, respectively, given in Eq. (2). Surface roughness was neglected in the calculations.

A. CsI Films

Figure 1 shows the near-normal reflectance of a 400-nm-thick CsI film. The curves in this and the following figures were drawn to connect data points. In the same figure we plot the normal reflectance of CsI crystals, calculated by use of Palik's compilation[15] of the optical constant data from Ref. 1. Table 1 shows the optical constants for as-deposited CsI films, as well as for films that were heated to 370 K for 5 h, then heated to 420 K for 2 h, and finally exposed to UV radiation for 8 h. The optical constant data for the as-deposited film are also shown in

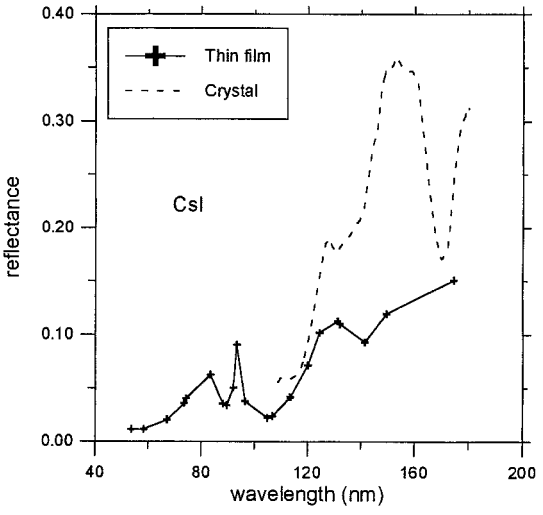

Fig. 1. Near-normal reflectance (5°) of a CsI film compared with the reflectance calculated with the optical constants of crystalline CsI.

Fig. 2. The error bars were calculated in terms of the uncertainty in the reflectance measurements (±2%), film thickness (±5 nm), degree of polarization (±0.05), and optical constants of the glass substrate (±0.05).

Heating the sample to 370 K had almost no effect on the optical constants of CsI. The further temperature increase to 420 K resulted in a decrease of the imaginary part of the refractive index k over the whole spectral range investigated, whereas the real part, n, did not change significantly. Exposing the sample to UV radiation resulted in a further decrease of k for wavelengths of 120.0 nm and longer, and a small increase of n for wavelengths longer than 113.5 nm. The sharp peak, exhibited by k at 93.2 nm for the as-deposited film, remained unchanged after heating to 370 K, but almost disappeared after further heating to 420 K. The peak of n at 96.4 nm also remained constant after heating the sample to 370 K, but decreased considerably after the subsequent heating to 420 K.

Figure 2 compares the current optical constants for the as-deposited CsI films to k data obtained from the absorption-length measurements by Boutboul *et al.*[12] and to the optical constant data for crystalline CsI compiled by Palik[15] from Ref. 1. For the wavelengths shorter than 109 nm we provide what to our knowledge is the first data for CsI optical constants in the literature. In the 109–125 -nm range our data and the data for crystalline CsI are close. At longer wavelengths, the optical constants n and k as well as the reflectance for the crystalline CsI are considerably higher than those for our thin films, which could be attributed to physical differences between CsI films and crystals, such as compactness, density, and surface morphology. The k values of Boutboul *et al.*[12] exceed the current data in the coincidence range (141.3–174.4 nm). This disagreement could possibly be due to the difference in film thickness, which is 400 nm for our films and 5–75 nm in Ref. 12. The optical

Table 1. Optical Constants (n, k) of As-Deposited and Treated CsI Films[a]

λ (nm)	n (a-d)[b]	k (a-d)	n (370)	k (370)	n (420)	k (420)	n (UV)	k (UV)
53.6	0.82 ± 0.02	0.19 ± 0.02	0.80 ± 0.02	0.15 ± 0.02	0.85 ± 0.02	0.08 ± 0.02		
58.4	0.82 ± 0.02	0.22 ± 0.02	0.79 ± 0.02	0.18 ± 0.02	0.87 ± 0.02	0.15 ± 0.02	0.89 ± 0.02	0.10 ± 0.02
67.1	0.83 ± 0.02	0.28 ± 0.02	0.77 ± 0.02	0.22 ± 0.02	0.84 ± 0.02	0.12 ± 0.02	0.87 ± 0.02	0.15 ± 0.02
73.5	0.84 ± 0.02	0.37 ± 0.02	0.79 ± 0.02	0.38 ± 0.02	0.84 ± 0.02	0.18 ± 0.02	0.87 ± 0.02	0.21 ± 0.02
74.3	0.85 ± 0.02	0.39 ± 0.02	0.77 ± 0.02	0.35 ± 0.02	0.81 ± 0.02	0.18 ± 0.02		
83.4	0.76 ± 0.02	0.39 ± 0.02	0.80 ± 0.02	0.49 ± 0.02	0.86 ± 0.02	0.27 ± 0.02		
87.9	1.00 ± 0.03	0.42 ± 0.02	0.97 ± 0.03	0.47 ± 0.02	0.93 ± 0.02	0.27 ± 0.02		
89.3	1.00 ± 0.02	0.41 ± 0.02	1.00 ± 0.03	0.47 ± 0.02	0.93 ± 0.02	0.27 ± 0.02		
92.0	0.89 ± 0.02	0.46 ± 0.02	0.85 ± 0.03	0.49 ± 0.02	0.81 ± 0.02	0.22 ± 0.02	0.86 ± 0.02	0.33 ± 0.02
93.2	0.92 ± 0.04	0.63 ± 0.02	0.80 ± 0.04	0.67 ± 0.02	0.80 ± 0.02	0.33 ± 0.02		
96.4	1.29 ± 0.03	0.39 ± 0.03	1.24 ± 0.04	0.47 ± 0.02	1.07 ± 0.02	0.31 ± 0.02		
104.8	1.03 ± 0.02	0.33 ± 0.02	1.09 ± 0.02	0.38 ± 0.02	0.96 ± 0.02	0.26 ± 0.02	1.03 ± 0.02	0.28 ± 0.02
106.7	1.02 ± 0.02	0.34 ± 0.02			0.94 ± 0.02	0.26 ± 0.02		
113.5	0.92 ± 0.02	0.42 ± 0.02	0.90 ± 0.02	0.32 ± 0.02	0.92 ± 0.02	0.33 ± 0.02	1.00 ± 0.02	0.29 ± 0.02
120.0	0.89 ± 0.03	0.55 ± 0.02	0.84 ± 0.02	0.37 ± 0.02	0.84 ± 0.02	0.38 ± 0.02	0.97 ± 0.02	0.28 ± 0.02
124.4	0.89 ± 0.03	0.66 ± 0.02	0.76 ± 0.02	0.41 ± 0.02	0.82 ± 0.02	0.48 ± 0.02	0.96 ± 0.02	0.32 ± 0.02
132.0	1.02 ± 0.04	0.75 ± 0.02			1.01 ± 0.04	0.66 ± 0.02	0.97 ± 0.02	0.46 ± 0.02
141.3	0.99 ± 0.04	0.67 ± 0.02			1.05 ± 0.03	0.58 ± 0.02		
149.4	1.14 ± 0.05	0.81 ± 0.02			1.12 ± 0.04	0.71 ± 0.02		
174.5	1.08 ± 0.05	0.91 ± 0.02			1.10 ± 0.05	0.85 ± 0.02		

[a]The films were later annealed to 370 ± 25 K for 5 h (370), later to 420 ± 25 K for 2 h (420), and then exposed to UV radiation for 8 h (UV).
[b]a-d, as deposited.

properties of thin films change for some materials with the film thickness, as for KBr films, which is mentioned in Subsection 3.C. The stoichiometry of the films, and hence their optical properties, can also be affected by molecular dissociation in the sublimation process. To minimize this effect, we deposited the CsI films, as well as the KI and KBr films, at a low temperature of the sublimating material.

B. KI Films

Figure 3 shows the near-normal reflectance of a 400-nm-thick KI film. In the same figure we plot the normal reflectance of a KI crystal calculated from Palik's optical constant compilation.[16] Table 2 shows the optical constants for the as-deposited KI films and also for the KI films that were heated to 370 K for 5 h, then heated to 420 K for 2 h, and finally exposed to UV radiation for 8 h. The optical constant data for the as-deposited films are also shown in Fig. 4. Heating the KI films to 420 K produced no significant change in the optical constants over the whole spectral range investigated. However, the exposure of the films to UV radiation had a pronounced effect on the optical constants. Extinction coefficient k of the sample exposed to UV radiation exhib-

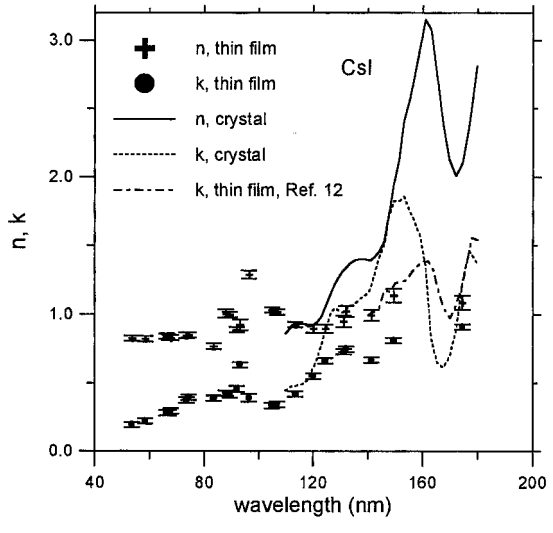

Fig. 2. Optical constants of CsI films compared with the data available in the literature for CsI crystals and for thin films (only k is available).

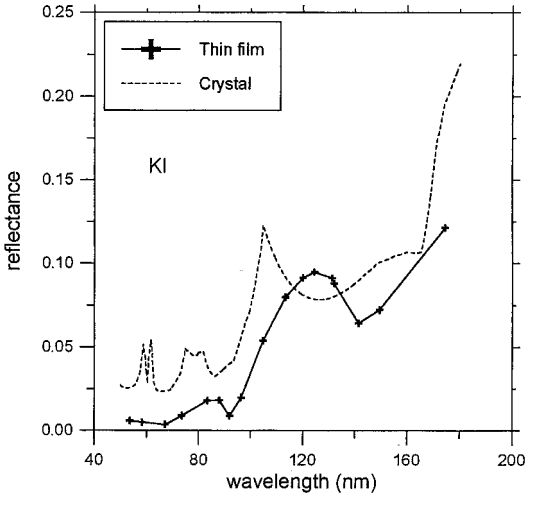

Fig. 3. Near-normal reflectance (5°) of a KI film compared with the reflectance calculated with the optical constants of crystalline KI.

Table 2. Optical Constants (n, k) of As-Deposited and Treated KI Films[a]

λ (nm)	n (a-d)[b]	k (a-d)	n (370)	k (370)	n (420)	k (420)	n (UV)	k (UV)
53.6	1.08 ± 0.02	0.18 ± 0.02	1.06 ± 0.02	0.18 ± 0.02	1.06 ± 0.02	0.18 ± 0.02	1.09 ± 0.02	0.17 ± 0.02
58.4	1.03 ± 0.02	0.23 ± 0.02	1.01 ± 0.02	0.23 ± 0.02	1.05 ± 0.02	0.25 ± 0.02	1.16 ± 0.02	0.13 ± 0.02
67.1	0.98 ± 0.02	0.14 ± 0.02	0.96 ± 0.02	0.13 ± 0.02	0.97 ± 0.02	0.15 ± 0.02	1.04 ± 0.02	0.14 ± 0.02
73.5	0.92 ± 0.02	0.21 ± 0.02	0.91 ± 0.02	0.20 ± 0.02	0.91 ± 0.02	0.21 ± 0.02	1.00 ± 0.02	0.13 ± 0.02
83.4	1.00 ± 0.02	0.30 ± 0.02	0.99 ± 0.02	0.27 ± 0.02	1.00 ± 0.02	0.28 ± 0.02	0.97 ± 0.02	0.22 ± 0.02
87.9	0.97 ± 0.02	0.27 ± 0.02	0.94 ± 0.02	0.24 ± 0.02	0.93 ± 0.02	0.25 ± 0.02	0.96 ± 0.02	0.28 ± 0.02
92.0	0.90 ± 0.02	0.25 ± 0.02	0.90 ± 0.02	0.24 ± 0.02	0.90 ± 0.02	0.25 ± 0.02	0.93 ± 0.02	0.32 ± 0.02
93.2			0.89 ± 0.02	0.24 ± 0.02	0.89 ± 0.02	0.24 ± 0.02	0.95 ± 0.02	0.33 ± 0.02
96.4	0.86 ± 0.02	0.25 ± 0.02	0.86 ± 0.02	0.27 ± 0.02	0.86 ± 0.02	0.26 ± 0.02	1.02 ± 0.02	0.40 ± 0.02
104.8	0.80 ± 0.02	0.41 ± 0.02	0.81 ± 0.02	0.42 ± 0.02	0.81 ± 0.02	0.43 ± 0.02	1.11 ± 0.02	0.31 ± 0.02
113.5	0.92 ± 0.03	0.58 ± 0.02	0.93 ± 0.03	0.59 ± 0.02	0.95 ± 0.03	0.62 ± 0.02	1.05 ± 0.02	0.29 ± 0.02
120.0	0.95 ± 0.03	0.63 ± 0.02	0.97 ± 0.04	0.65 ± 0.02	0.99 ± 0.04	0.67 ± 0.02	1.00 ± 0.02	0.30 ± 0.02
124.4	1.00 ± 0.04	0.66 ± 0.02	0.98 ± 0.04	0.67 ± 0.02	1.02 ± 0.04	0.70 ± 0.02	0.96 ± 0.02	0.31 ± 0.02
132.0	1.11 ± 0.04	0.68 ± 0.02	1.10 ± 0.04	0.69 ± 0.02	1.12 ± 0.04	0.70 ± 0.02	1.14 ± 0.03	0.57 ± 0.02
141.3	1.14 ± 0.03	0.55 ± 0.02	1.14 ± 0.03	0.57 ± 0.02	1.13 ± 0.03	0.57 ± 0.02	1.18 ± 0.02	0.40 ± 0.02
149.4	1.10 ± 0.03	0.60 ± 0.02	1.09 ± 0.04	0.62 ± 0.02	1.12 ± 0.04	0.62 ± 0.02	1.12 ± 0.02	0.37 ± 0.02
174.5	1.15 ± 0.05	0.82 ± 0.02	1.13 ± 0.05	0.84 ± 0.02	1.16 ± 0.05	0.85 ± 0.02	1.34 ± 0.04	0.50 ± 0.03

[a]The films were later annealed to 370 ± 25 K for 5 h (370), later to 420 ± 25 K for 2 h (420), and then exposed to UV radiation for 8 h (UV).
[b]a-d, as deposited.

ited completely different values for wavelengths of 92.0 nm and longer, whereas its maximum at 132.0 nm disappeared. Refractive index n was higher than that for the as-deposited and for the heated films over the whole spectral range, with a maximum located at 92.0 nm, just where n had a minimum for both the as-deposited and the heated film. Figure 4 compares the optical constants of crystals and as-deposited films. The crystal data were presented in Refs. 3 and 4 and are summarized in Ref. 16. There is a reasonable qualitative as well as quantitative agreement between these optical constants. The largest difference is for n in the short- and long-wavelength extremes. In Fig. 3 there is a more important disagreement in the normal incidence reflectance. Similar to CsI, the different optical properties of KI can be attributed to physical differences between films and crystals. The discrete set of wavelengths available in our reflectometer did not allow resolution of the different peaks observed in the literature for the optical constants of KI crystals.

C. KBr Films

In the case of KBr films, we selected a film thickness of 100 nm because it maximized the measured EUV reflectance. Figure 5 shows the near-normal reflectance measured for a 100-nm-thick KBr film. In the same figure we plot the normal reflectance of KBr calculated with the optical constants from Refs. 3, 4, and 7 and summarized in Palik's compilation.[17] There is a remarkable agreement between the film

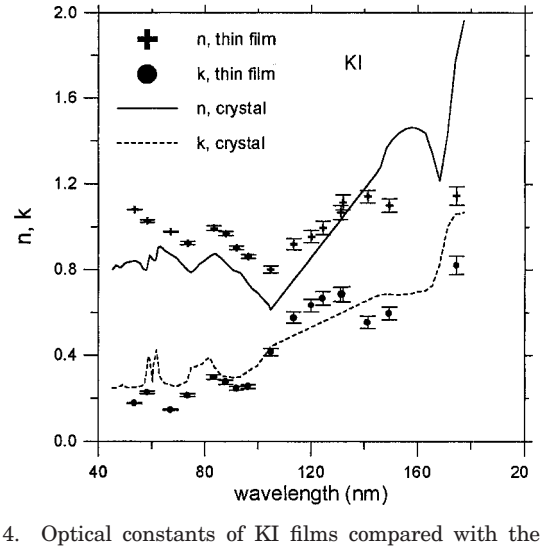

Fig. 4. Optical constants of KI films compared with the data available in the literature for KI crystals.

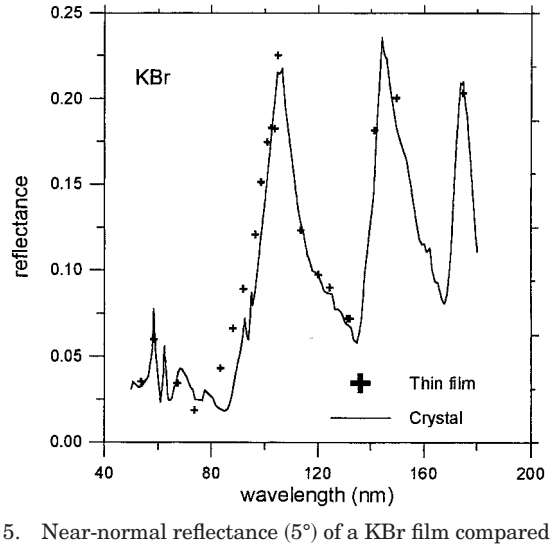

Fig. 5. Near-normal reflectance (5°) of a KBr film compared with the reflectance calculated with the optical constants of crystalline KBr.

Table 3. Optical Constants (n, k) of As-Deposited KBr Films[a]

λ (nm)	n (a-d)[b]	k (a-d)	n (420)	k (420)	n (UV)	k (UV)
53.6	0.87 ± 0.02	0.28 ± 0.02	0.93 ± 0.02	0.31 ± 0.02	0.95 ± 0.02	0.35 ± 0.02
58.4	1.00 ± 0.03	0.51 ± 0.02	0.96 ± 0.02	0.44 ± 0.02	1.05 ± 0.03	0.52 ± 0.02
67.1	0.88 ± 0.02	0.30 ± 0.02	0.93 ± 0.02	0.34 ± 0.02	0.91 ± 0.02	0.35 ± 0.02
73.5	1.00 ± 0.02	0.26 ± 0.02	1.01 ± 0.02	0.25 ± 0.02	1.05 ± 0.02	0.27 ± 0.02
83.4	0.86 ± 0.02	0.34 ± 0.02	0.92 ± 0.02	0.35 ± 0.02	0.97 ± 0.02	0.40 ± 0.02
87.9	0.76 ± 0.02	0.35 ± 0.02	0.80 ± 0.02	0.38 ± 0.02	0.84 ± 0.02	0.44 ± 0.02
92.0	0.72 ± 0.02	0.43 ± 0.02	0.72 ± 0.02	0.39 ± 0.02	0.74 ± 0.02	0.47 ± 0.02
96.4	0.74 ± 0.02	0.56 ± 0.02	0.76 ± 0.03	0.55 ± 0.02	0.80 ± 0.03	0.61 ± 0.02
98.5	0.76 ± 0.03	0.68 ± 0.02				
100.9	0.81 ± 0.04	0.80 ± 0.02	0.79 ± 0.04	0.73 ± 0.02	0.87 ± 0.04	0.81 ± 0.02
102.5	0.88 ± 0.05	0.86 ± 0.02	0.88 ± 0.04	0.79 ± 0.02	0.87 ± 0.05	0.85 ± 0.02
103.7	0.94 ± 0.05	0.92 ± 0.02	0.93 ± 0.05	0.85 ± 0.02	1.00 ± 0.05	0.93 ± 0.02
104.8	0.92 ± 0.06	1.03 ± 0.02	0.81 ± 0.04	0.89 ± 0.02	0.95 ± 0.06	1.03 ± 0.02
113.5	1.36 ± 0.06	0.81 ± 0.02	1.32 ± 0.06	0.81 ± 0.02	1.17 ± 0.05	0.84 ± 0.02
120.0	1.32 ± 0.05	0.69 ± 0.02	1.28 ± 0.05	0.68 ± 0.02	1.21 ± 0.05	0.71 ± 0.02
124.4	1.23 ± 0.04	0.67 ± 0.02	1.18 ± 0.04	0.64 ± 0.02	1.37 ± 0.05	0.65 ± 0.03
132.0	1.10 ± 0.03	0.57 ± 0.02	1.11 ± 0.03	0.57 ± 0.02	1.27 ± 0.04	0.59 ± 0.02
141.3	0.87 ± 0.04	0.86 ± 0.02	0.89 ± 0.04	0.86 ± 0.02	0.92 ± 0.05	0.91 ± 0.02
149.4	1.47 ± 0.08	1.16 ± 0.02	1.37 ± 0.07	1.09 ± 0.02	1.47 ± 0.08	1.16 ± 0.02
174.5	1.58 ± 0.08	1.18 ± 0.03			1.57 ± 0.08	1.22 ± 0.03

[a]The films were later annealed to 420 ± 25 K for 2 h (420) and then exposed to UV radiation for 8 h (UV).
[b]a-d, as deposited.

and the crystal reflectance, in contrast with the above data for CsI and KI. Table 3 shows the optical constants for the as-deposited KBr films and also for the KBr films that were heated to 420 K for 2 h, and then exposed to UV radiation for 8 h. The optical constant data for the as-deposited KBr films are also shown in Fig. 6.

As mentioned above, the 50–100-nm-thick KBr films exhibited a higher EUV and FUV normal reflectance than the 400-nm-thick films. This difference might be attributed to a smoother and/or more compact structure of the 50–100-nm-thick films, which were therefore selected for the optical constant determination. The optical constants of KBr did not change significantly after either heating the samples to 420 K or exposing them to UV irradiation. The only considerable change was in the peak of n at 113.5 nm for the as-deposited and the heated films, which shifted to 124.4 nm for the UV-irradiated films.

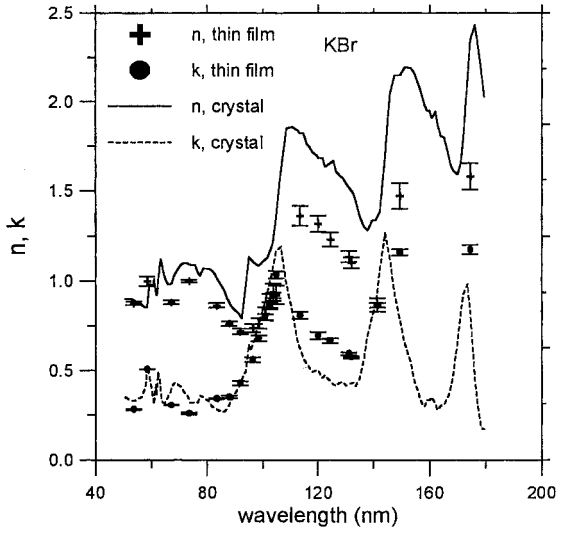

Fig. 6. Optical constants of KBr films compared with the data available in the literature for KBr crystals.

Figure 6 compares the optical constant data of the as-deposited films and of the crystals. Crystal data were taken from Ref. 17, which summarizes the results of Refs. 3, 4, and 7. Both data sets show a considerable qualitative agreement, although there are large quantitative differences, which could arise from possible physical differences between films and crystals. Again, the discrete set of wavelengths available in our reflectometer did not allow resolution of all the different peaks that were observed in the literature for the optical constants of KBr crystals.

4. Quantum Efficiency of Planar Reflective Photocathodes

A. Quantum Efficiency Variation with Heating and UV Irradiation

Here we describe the measurements of QE for planar reflective CsI, KI, and KBr photocathodes, which were carried out in the Space Sciences Laboratory at the University of California at Berkeley. In this study we compared the experimental data for QE variation with heating and UV irradiation with the results of our theoretical calculations based on the measured optical constants. The experimentally measured absolute values of QE of the as-deposited CsI, KI, and KBr photocathodes obtained at normal incidence are shown in Fig. 7. Following these measurements, we heat treated or UV irradiated the pho-

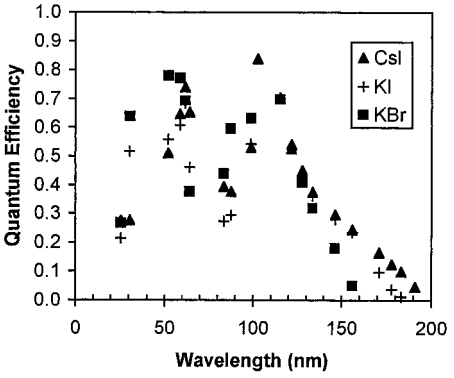

Fig. 7. QE of CsI, KBr, and KI planar reflective photocathodes as a function of wavelength.

tocathode samples and subsequently remeasured their QE after each treatment.

The relative variation of the photocathode sensitivity after heat treatment is shown in Fig. 8(a). The QE of the KI and KBr photocathodes remained almost unchanged after heat annealing, whereas the QE of the CsI photocathode increased by ≈20% at 180 nm. The data of Boutboul *et al.*[12,18] showed that heat annealing did not result in any variation of the absorption length and of the electron escape length in CsI photocathodes. The fact that these two parameters have not changed suggests that CsI QE has changed in our samples because postevaporation heating either lowered the electron affinity or induced the removal of residual water and/or other molecules from the surface, which improved the electron emission. However, the desorption of water molecules, mentioned as one of the reasons for the sensitivity increase,[12] cannot solely explain the QE enhancement. Otherwise KI, which is the most sensitive to water-vapor exposure among the materials studied, should have exhibited the largest increase in sensitivity.

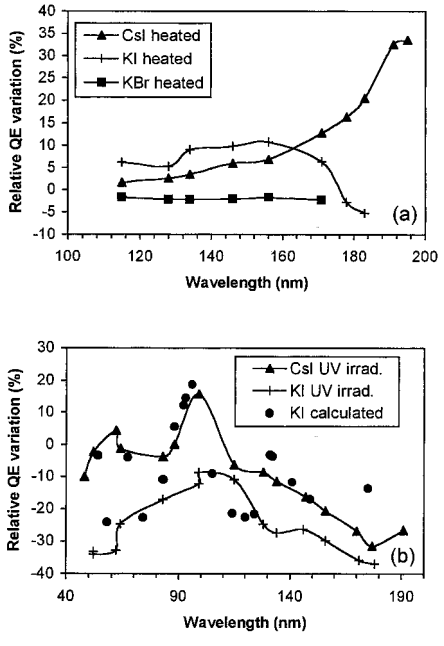

Fig. 8. (a) Relative variation of QE measured after the samples were heated to 370 K (normalized to the as-deposited QE values). (b) Relative variation of QE measured with UV-irradiated photocathodes (normalized to the QE values measured before irradiation). The experimentally measured QE changes were obtained with samples irradiated by an UV flux of 1.15×10^{10} photons mm^{-2} sec^{-1} at 253.7 nm with a total dose of 8×10^{14} photons. The calculated QE variation of the KI photocathode was obtained with the current optical constants measured for UV-irradiated KI films.

Figure 8(b) represents the QE relative variation after the samples were UV irradiated. The sensitivity of UV-irradiated CsI and KI photocathodes was reduced considerably, whereas in KBr samples (not shown) the degradation was not as pronounced. A detailed study of the stability of alkali-halide photocathodes under UV irradiation can be found elsewhere.[19–24]

A previous study of the crystalline structure of fresh and UV-irradiated CsI photocathodes with the help of transmission electron microscopy[23] demonstrated that evaporated films have a polycrystalline structure. Furthermore, we did not observe any change in the CsI film surface morphology or crystalline structure after it was exposed to 10^{15} photons/mm^2 irradiation with 253.7-nm photons. However, the decay of the CsI films under an electron-beam bombardment appeared to be more pronounced for the UV-irradiated samples. We assumed the latter fact could be explained by the presence of color centers in the irradiated samples, which, in turn, increased the trapping of the bombarding electrons.

Here we try to correlate the variation of the film optical constants described above with the reduction of the photocathode efficiency. We calculated the variation of the KI photocathode quantum efficiency assuming that only the optical constants changed after the samples were UV irradiated. The model we used for these calculations is based on the photocathode QE model suggested by Fraser,[25] and it is described in detail in Ref. 26. For the calculations we used the optical constants of the as-deposited and UV-irradiated film that were presented in Section 3. We assumed that the photoelectron excitation, transport, and escape parameters did not change with photocathode aging under UV irradiation. By assuming that the photoelectron parameters remain constant and by comparing the calculated results with the measured data, we can determine whether the variation of the optical constants can solely explain the sensitivity reduction or the electron transport properties are also modified by UV exposure. The circles in Fig. 8(b) represent the results of our calculations for the KI photocathode QE variation with UV irradiation. The observed discrepancies between the calculated and the measured data, shown in Fig. 8(b), revealed that the changes in the optical properties of photocathodes cannot solely explain the observed QE changes after heating and UV irradiation, but the variation of the electron transport properties should also be taken into account. At the same time, the

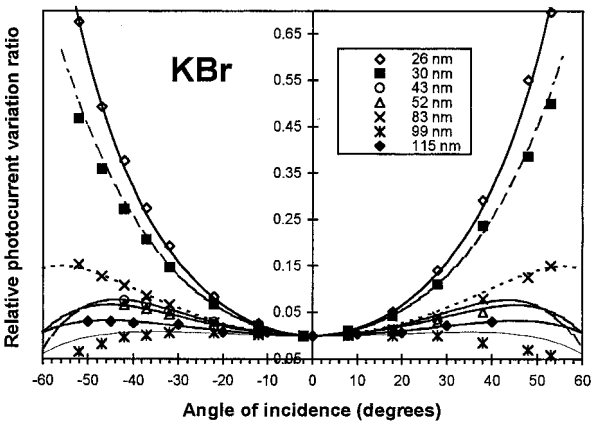

Fig. 9. Angular variation of KBr photocathode quantum efficiency at different wavelengths normalized to the efficiency at normal incidence. The separate points correspond to the experimental data. The curves represent the results of theoretical calculations.

angular response of the photocathodes was simulated with the measured optical constants, and it is presented in Subsection 4.B. The formation of color centers, which changes both the UV absorption coefficient and the photoelectron escape length, can present a possible explanation for the sensitivity degradation under UV illumination.

B. Angular Variation of Photocathode Sensitivity: Measurements and Calculations

Variation of the photocathode QE with the incidence angle can result in significant nonlinearities in response of imaging and spectroscopic devices (see, e.g., Ref. 27). We experimentally measured the QE variation of KBr photocathodes with the angle of radiation incidence in the 25–115-nm spectral range and compared these data with the results of our theoretical calculations, based on the model suggested by Fraser.[25] The comparison is shown in Fig. 9. The model calculates the probability of photon absorption at a particular depth in the photocathode, the probability of producing a photoelectron, and then the probability of this photoelectron to escape back into vacuum. The optical constants for these calculations were taken from the measurements described above and from Ref. 17. A detailed description of our calculations can be found in Ref. 28. The results of theoretical calculations of the photocathode angular response are in a good agreement with the measured data, which validates the optical constants reported in Section 3. We have shown that the angular response of alkali-halide photocathodes can be estimated if both the optical constants and the electron transport parameters are known for a particular material. Optimization of the detection device parameters in terms of incidence angles can substantially improve the efficiency of the space-flight instruments. For example, the bias angle in microchannel plates in the Galaxy Evolution Explorer (GALEX) NASA flight detector was chosen to be 19° to optimize the detection efficiency of the device.[29]

5. Conclusions

We obtained the optical constants for thin films of CsI, KI, and KBr in the FUV and EUV spectral ranges, in which only the optical constants of crystalline CsI, KI, and KBr were previously available. At wavelengths shorter than 112.7 nm no optical constant of CsI in any form was previously available. The optical constants of thin films of KI and KBr showed reasonable agreement with the crystal data. However, there was considerable disagreement between the thin-film and the crystalline data for CsI at wavelengths for which crystal data were available. In our opinion, the observed differences in the optical constants of the thin film and crystal are likely to be explained by physical differences between films and crystals, such as compactness, density, and surface morphology.

Samples of the three materials were exposed *in situ* to thermal treatment and UV irradiation. Among the three photocathode materials investigated, KBr was the most stable to thermal treatment and UV irradiation. Its optical constants were barely affected by the treatments, whereas those for KI thin film exhibited the largest change after exposure to UV radiation. The optical constants of CsI film changed after both heating and UV irradiation. We observed a correlation between the changes in optical constants and QE of thin-film photocathodes: CsI exhibited the largest change both in optical constants and in QE with heating and UV irradiation, whereas KBr was the most stable among the studied materials. However, the QE variation of these photocathodes cannot be explained solely by changes in their optical constants after UV irradiation and heat treatment. A combination of changes in the optical properties and in the electron transport properties of these materials is likely to be responsible for the observed sensitivity variation. The results of our angular QE variation studies showed that the optical constants reported in this paper proved to be useful for the estimation of sensitivity variation with the angle of radiation incidence.

We acknowledge Joaquín Campos Acosta for the optical calibration of the Hg–Xe lamp and José M. Sánchez-Orejuela for his technical assistance.

References

1. K. I. Saïd and G. W. Green, "Optical properties of caesium iodide in the vacuum ultraviolet," J. Phys. C **10,** 479–488 (1977).
2. H. R. Philipp and H. Ehrenreich, "Intrinsic optical properties of alkali halides," Phys. Rev. **131,** 2016–2022 (1963).
3. D. Blechschmidt, R. Klucker, and M. Skibowski, "Dielectric properties of KCl, KBr, and KI single crystals in the extreme ultraviolet up to 35 eV," Phys. Status Solidi **36,** 625–634 (1969).
4. T. Tomiki, T. Miyata, and H. Tsukamoto, "Temperature dependence of the fundamental spectra of potassium-halides in

the Schumann ultraviolet region (4.4–13.5 eV)," J. Phys. Soc. Jpn. **35,** 495–507 (1973).
5. T. Tomiki, T. Miyata, and H. Tsukamoto, "The Urbach rule for the sodium- and potassium-halides," Z. Naturforsch. Teil A **29,** 145–147 (1974).
6. G. Stephan, É. Garignon, and S. Robin, "Spectres électroniques du KBr dans l'ultraviolet extrême," C. R. Acad. Sci. Ser. B **268,** 408–411 (1969).
7. M. Antinori, A. Balzarotti, and M. Piacentini, "High-resolution reflection spectra of alkali halides in the far ultraviolet," Phys. Rev. B **7,** 1541–1549 (1973).
8. J. E. Eby, K. J. Teegarden, and D. B. Button, "Ultraviolet absorption of alkali halides," Phys. Rev. **116,** 1099–1105 (1959).
9. K. Teegarden and G. Baldini, "Optical absorption spectra of the alkali halides at 10° K," Phys. Rev. **155,** 896–907 (1967).
10. H. Saito, S. Saito, and R. Onaka, "Extreme ultraviolet absorption of alkali halides," J. Phys. Soc. Jpn. **24,** 1095–1098 (1968).
11. C. Lu and K. T. McDonald, "Properties of reflective and semitransparent CsI photocathodes," Nucl. Instrum. Methods Phys. Res. A **343,** 135–151 (1994).
12. T. Boutboul, A. Breskin, R. Chechik, A. Braem, and G. Lion, "Ultraviolet photoabsorption measurements in alkali iodide and caesium bromide evaporated films," J. Appl. Phys. **83,** 7896–7899 (1998).
13. J. I. Larruquert, J. A. Aznárez, and J. A. Méndez, "FUV reflectometer for *in-situ* characterization of thin films deposited under UHV," in *Instrumentation for UV/EUV Astronomy and Solar Missions,* S. Fineschi, C. M. Korendyke, O. H. W. Siegmund, and B. E. Woodgate, eds., Proc. SPIE **4139,** 92–101 (2000).
14. J. A. Aznárez, J. I. Larruquert, and J. A. Méndez, "Far-ultraviolet absolute reflectometer for optical constant determination of ultrahigh vacuum prepared thin films," Rev. Sci. Instrum. **67,** 497–502 (1996).
15. J. E. Eldridge, Cesium Iodide (CsI), in *Handbook of Optical Constants of Solids, Vol. 2*, E. D. Palik, ed. (Academic San Diego, Calif., 1991).
16. M. E. Thomas, "Potassium Iodide (KI)," in *Handbook of Optical Constants of Solids, Vol. 3*, E. D. Palik, ed. (Academic, San Diego, Calif., 1998).
17. E. D. Palik, "Potassium bromide (KBr)," in *Handbook of Optical Constants, Vol. 2*, E. D. Palik, ed. (Academic, San Diego, Calif., 1991).
18. T. Boutboul, A. Akkerman, A. Breskin, and R. Chechik, "Escape length of ultraviolet induced photoelectrons in alkali iodide and CsBr evaporated films: measurements and modeling," J. Appl. Phys. **84,** 2890–2896 (1998).
19. A. Breskin, "CsI UV photocathodes: history and mystery," Nucl. Instrum. Methods Phys. Res. A **371,** 116–136 (1996).
20. A. Lu, Z. Cheng, D. R. Marlow, K. T. McDonald, E. J. Prebys, I. H. Stairs, R. L. Wixted, I. Adachi, R. Itoh, T. Sumiyoshi, N. S. Lockyer, and J. E. Millan, "Prototype studies of a fast RICH detector with a CsI photocathode," Nucl. Instrum Methods Phys. Res. A **371,** 155–161 (1996).
21. J. Vavra, A. Breskin, A. Buzulutskov, R. Chechik, and E. Shefer, "Study of CsI photocathodes: volume resistivity and aging," Nucl. Instrum. Methods Phys. Res. A **387,** 154–162 (1997).
22. A. S. Tremsin and O. H. W. Siegmund, "Heat enhancement of radiation resistivity of evaporated CsI, KI, and KBr photocathodes," Nucl. Instrum. Methods Phys. Res. A **442,** 337–341 (2000).
23. A. S. Tremsin, S. Ruvimov, and O. H. W. Siegmund, "Structural transformation of CsI thin film photocathodes under exposure to air and UV irradiation," Nucl. Instrum. Methods Phys. Res. A **447,** 614–618 (2000).
24. A. S. Tremsin and O. H. W. Siegmund, "UV radiation resistance and solar blindness of CsI and KBr photocathodes," IEEE Trans. Nucl. Sci. **48,** 481–425 (2001).
25. G. W. Fraser, "The characterisation of soft X-ray photocathodes in the wavelength band 1–300 Å," Nucl. Instrum. Methods Phys. Res. **206,** 251–263 (1983).
26. J. I. Larruquert, J. A. Méndez, J. A. Aznárez, A. S. Tremsin, and O. H. W. Siegmund, "Optical constants of as-deposited and treated alkali halides and their VUV quantum efficiency," in *EUV, X-Ray, and Gamma-Ray Instrumentation for Astronomy X*, O. H. W. Siegmund and K. A. Flanagan, eds., Proc. SPIE **3765,** 789–798 (1999).
27. S. M. Johnson, Jr., "Ultraviolet angular response of cesium–telluride photocathodes," Appl. Opt. **31,** 2332–2342 (1992).
28. A. S. Tremsin and O. H. W. Siegmund, "Dependence of quantum efficiency of alkali halide photocathodes on the radiation incidence angle," in *EUV, X-Ray, and Gamma-Ray Instrumentation for Astronomy X*, O. H. W. Siegmund and K. A. Flanagan, eds., Proc. SPIE **3765,** 441–451 (1999).
29. O. H. W. Siegmund, P. N. Jelinsky, S. R. Jelinsky, J. M. Stock, J. S. Hull, D. L. Doliber, J. Zaninovich, A. S. Tremsin, and K. E. Kromer, "High-resolution cross delay line detectors for the GALEX mission," in *EUV, X-Ray, and Gamma-Ray Instrumentation for Astronomy X*, O. H. W. Siegmund and K. A. Flanagan, eds., Proc. SPIE **3765,** 429–440 (1999).